JPE 16-6-13

http://dx.doi.org/10.6113/JPE.2016.16.6.2119
ISSN(Print): 1598-2092 / ISSN(Online): 2093-4718

A Study of the SPWM High-Frequency Harmonic Circulating Currents in Modular Inverters

Sheng Xu† and Zhendong Ji*

†Department of Mechanical and Electrical Engineering, Taizhou University, Taizhou, China
*School of Automation, Nanjing University of Science and Technology, Nanjing, China

Abstract

Due to detection and control errors, some high-frequency harmonics with voltage-source characteristics cause circulating currents in modular inverters. Moreover, the circulating currents are usually affected by the output filters (OF) of each module due to their filter and resonance properties. The interaction among the circulating currents in the modules increase the power loss and reduce system stability and control precision. Therefore, this paper reports the results of a study on the SPWM high-frequency harmonics circulating currents for a double-module VSI. In the paper, an analysis of the circulating-current circuits is briefly described. Next, a mathematic model of the single-module output voltage based on the carrier frequency of SPWM is built. On this basis, through mathematic modeling of high-frequency harmonic circulating currents, the formation mechanism and distribution characteristics of circular currents and their influences are studied in detail. Finally, the influences of the OF on the circulating currents are studied by mainly taking an LC-type filter as an example. A theoretical analysis and experimental results demonstrate some important characteristics. First, the carrier phase shifting of the SPWM for each module is the major cause of the SPWM harmonic circulating currents, and the circulating currents are in an odd distribution around n-times the carrier frequency $n\omega_s$, where n = 1, 2, 3, …. Second, the harmonic circular currents do not flow into the parallel system. Third, the OF can effectively suppress the non-circulating part of the high-frequency harmonic currents but is ineffective for the circulation part, and actually reduces system stability.

Key words: High-frequency harmonic circulating currents, output filter, Modular inverters, SPWM

I. INTRODUCTION

The problem of circulating currents in modular inverters has gained widespread attention in recent years. Studies of these circulating currents mainly include two directions: 1) fundamental active and reactive circulating currents [1] and 2) harmonic circulating currents [2]. The former studies mainly focused on micro-grid inverters [3], [4] and uninterruptible power supplies [5]. In addition, the fundamental circulating currents are generally caused by amplitude, phase and frequency errors of the output voltage of each power module. Many common load-sharing control approaches, such as the instantaneous average-current-sharing method [6], [7], the droop control method and improved methods [8]-[11] based on virtual impedances, are adopted to restrain the fundamental circulating currents.

In contrast, few studies exist on harmonic circulating currents. However, with the continuing increases in inverter quality requirements, the harmonic circulating-current problem will become more prominent. The main cause of harmonic circulating currents is the generation of some harmonics via detection and control errors between the power modules, which do not have the characteristics of a controlled current source. For example, the dead-time differences of power switches [12], [13] and the carrier phase shifting of the SPWM between each inverter module cause harmonic circulating currents [14], [15].

In addition, some type of output filter (OF) such as an LC-type filter is typically required at the output side of an inverter to filter the high-frequency harmonic currents produced by the inverter. However, some experimental results have shown that differences in the type and parameters of the OF result in dissimilar characteristics of the

Manuscript received Feb. 5, 2016; accepted Jul. 22, 2016
Recommended for publication by Associate Editor Younghoon Cho.
†Corresponding Author:xush_00@sina.com
Tel: +86-523-80769043, Fax: +86-523-80769280, Taizhou University
*School of Automation, Nanjing Univ. of Science and Tech., China

high-frequency circulating currents. In fact, the filtering and resonance characteristics of an OF inevitably impact the properties of high-frequency circulating currents [16], [17].

This paper focuses on a study of SPWM high-frequency harmonic circulating currents using the quantitative analysis method and considering the case of double-module inverters. First, the high-frequency switching circulating-current circuits of a modular inverter are briefly analyzed. Next, a mathematical model of the single-module output voltage based on the SPWM carrier frequency is built. On this basis, through the construction of a mathematical model of the high-frequency harmonic circulating currents, the formation mechanism and the distribution characteristics of the circulating currents and their impact on parallel systems are analyzed in detail. Finally, the influences of the OF on the circulating currents, taking an LC-type filter and an LCL-type filter as examples, are studied.

II. HIGH-FREQUENCY SWITCHING CIRCULATING-CURRENT CIRCUITS

To reveal the formation mechanism of the high-frequency switching harmonic circulating currents from the power switch level, this paper analyses the formation paths of the circulating currents, taking a double-module VSI as an example. Fig. 1 is a simplified switching circuit model of a double-module VSI.

In Fig. 1, S_{kij} is the equivalent switch and L_{ki} is the input connection inductor of each inverter module, where k = a, b and c; i = 1 and 2; and j = p and n. The module's DC Power supplies are denoted as U_{dc1} and U_{dc2} for module 1 and module 2, respectively.

The switching circulating current formation paths are demonstrated according to the switching combination states of the modular inverters. The switching state functions are defined as S_{a1}, S_{b1}, S_{c1}, S_{a2}, S_{b2} and S_{c2} for each bridge arm of the VSI. Taking S_{a1} as an example, S_{a1} = 1 indicates that S_{a1p} is turned on and S_{a1n} is switched off. Conversely, S_{a1} = 0 indicates that S_{a1p} is switched off and S_{a1n} is turned on. Similar meanings are applied to the other switching state functions.

There are 64 types of switching combinations in total. Due to space limitations, only the typical switching combination states are analyzed according to all of types of the high-frequency circulating-current characteristics.

First, the circulating-current circuits do not contain U_{dc1} and U_{dc2}. In this case, the switching combination $S_{a1}S_{b1}S_{c1}S_{a2}S_{b2}S_{c2}$ includes four types of states, which are 111111, 000000, 111000 and 000111. Correspondingly, one of the circulating-current circuits is: $S_{a1p}\rightarrow L_{a1}\rightarrow L_{a2}\rightarrow S_{a2p}\rightarrow S_{b2p}\rightarrow L_{b2}\rightarrow L_{b1}\rightarrow S_{b1p}\rightarrow S_{a1p}$.

Second, U_{dc1} and U_{dc2} exist in the circulating-current circuits in series with opposite directions. In such a case, the feature of the switching combination states is $S_{a1}S_{b1}S_{c1} = S_{a2}S_{b2}S_{c2}$, such as 111111 and 000000. Taking the switching combination 001001 as an example, there are two circulating-current circuits as follows: $U_{dc1}^{+}\rightarrow S_{c1p}\rightarrow L_{c1}\rightarrow L_{c2}\rightarrow S_{c2p}\rightarrow U_{dc2}^{+}\rightarrow U_{dc2}^{-}\rightarrow S_{a2n}\rightarrow L_{a2}\rightarrow L_{a1}\rightarrow S_{a1n}\rightarrow U_{dc1}^{-}$ and $U_{dc1}^{+}\rightarrow S_{c1p}\rightarrow L_{c1}\rightarrow L_{c2}\rightarrow S_{c2p}\rightarrow U_{dc2}^{+}\rightarrow U_{dc2}^{-}\rightarrow S_{b2n}\rightarrow L_{b2}\rightarrow L_{b1}\rightarrow S_{b1n}\rightarrow U_{dc1}^{-}$. Obviously, the total power value of this type of circulating-current circuit is U_{dc1}-U_{dc2}.

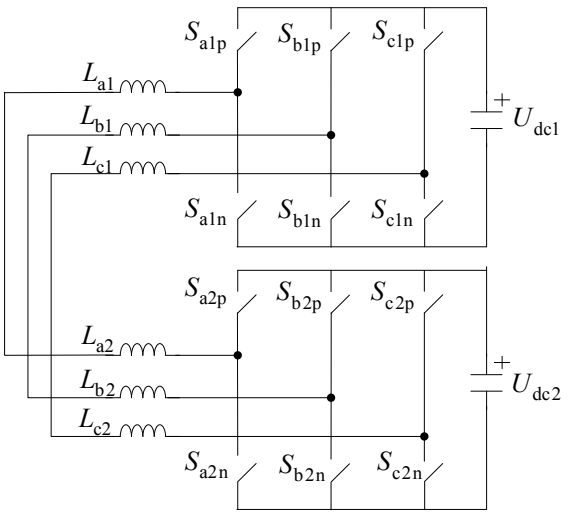

Fig. 1. Simplified switching circuit model of a double-module VSI.

Third, the circulating-current circuits only contain one of the two DC supplies: U_{dc1} or U_{dc2}. Taking the case of the switching combination 000001, the two circulating-current circuits are as follows: $U_{dc2}^{+}\rightarrow S_{c2p}\rightarrow L_{c2}\rightarrow L_{c1}\rightarrow S_{c1n}\rightarrow S_{a1n}\rightarrow L_{a1}\rightarrow L_{a2}\rightarrow S_{a2n}\rightarrow U_{dc2}^{-}$ and $U_{dc2}^{+}\rightarrow S_{c2p}\rightarrow L_{c2}\rightarrow L_{c1}\rightarrow S_{c1n}\rightarrow S_{b1n}\rightarrow L_{b1}\rightarrow L_{b2}\rightarrow S_{b2n}\rightarrow U_{dc2}^{-}$.

Fourth, the circulating-current circuits contain U_{dc1} and U_{dc2} in series with the same direction. That is, the total power value of this kind of circulating-current circuit is U_{dc1}+U_{dc2}. Taking the switching combination 000001 as an example, the circulating-current circuit is: $U_{dc1}^{+}\rightarrow S_{c1p}\rightarrow L_{c1}\rightarrow L_{c2}\rightarrow S_{c2p}\rightarrow U_{dc2}^{-}\rightarrow U_{dc2}^{+}\rightarrow S_{b2p}\rightarrow L_{b2}\rightarrow L_{b1}\rightarrow S_{b1n}\rightarrow U_{dc1}^{-}$.

In short, according to the above analysis, the following conclusions can be made. First, the circulating-current circuits can be divided into four types in accordance with the series DC power value. Second, the formation of the circulating currents depends on the switching status of the parallel modules along with the magnitude and the change rate of the circulating currents determined by the input reactance and the DC supply voltages in series in the circulating-current circuits.

III. MATHEMATICAL MODELING OF THE OUTPUT PHASE VOLTAGE OF THE INVERTER MODULE BASED ON THE SPWM CARRIER FREQUENCY

A. Structure of a Modular Inverter

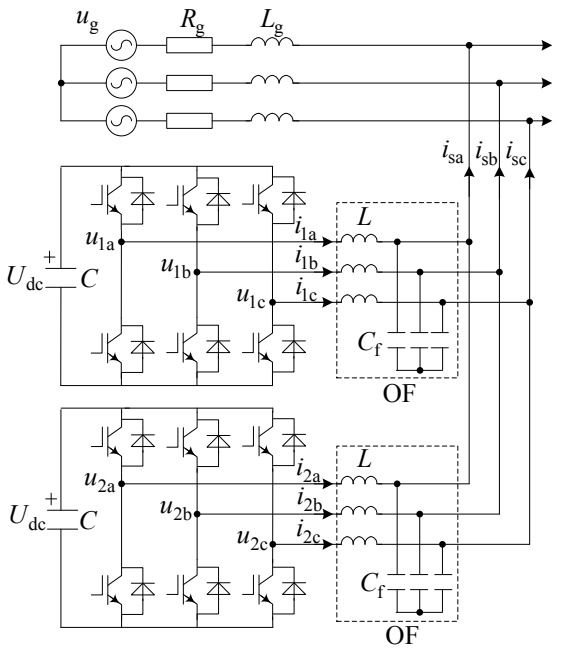

Fig. 2. The main circuit structure of the double-module VSI with an LC-type OF.

Fig. 2 shows the main circuit structure of a double-module VSI with an LC-type OF. In Fig. 2, u_g is the power supply voltage, R_g and L_g are the grid equivalent resistance and reactance, respectively, and the reactance L and capacitance C_f are the components of the LC filter. In addition, the three-phase output currents and phase voltages of each module and the three-phase parallel system currents are denoted as i_{kx}, u_{kx} and i_{sx}, respectively, where k = 1 and 2, and x = a, b and c.

For the purpose of simplifying the analysis of the high-frequency harmonic circulating currents, the parallel system here is set with the following characteristics. First, the three-phase power supply voltages are sinusoidal and balanced. Second, each module has the same component parameters, DC voltage and SPWM modulation waveform. Third, the reference potential of the module output phase voltages is selected in the point of half of the DC capacitor C instead of the negative terminal of the C, to avoid the DC voltage component from being involved in the phase voltages. In addition, due to the symmetry of three-phase systems, the phase A is considered for the problem analysis, and the subscript 'a' is omitted.

B. Mathematical Modeling of the Module's Output Phase Voltage

To accurately analyze the formation mechanism of the harmonic circulating currents, a mathematical model of the module's output phase voltage is built based on the SPWM carrier frequency.

Let the output phase voltage be comprised of n times harmonics. According to the linear superposition principle, any single harmonic voltage may be taken as an analysis object.

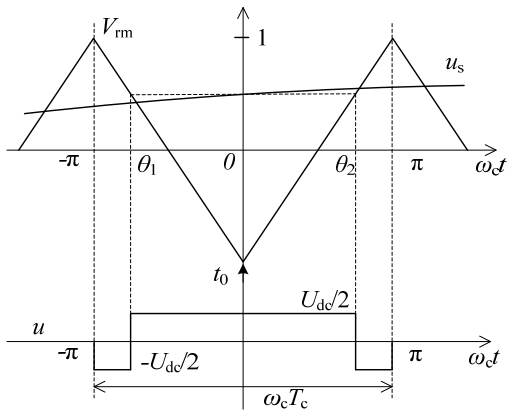

Fig. 3. The output phase voltage in one switching cycle based on the regular sampling method.

Fig. 3 shows the output phase voltage in one switching cycle T_c based on the regular sampling method.

In Fig. 3, ω_c and V_{rm} represent the frequency and amplitude of the carrier wave, and the voltage modulation wave is denoted as u_s, which is given as follows:

$$u_s = U_m \sin(\omega_s t + \varphi) \tag{1}$$

Referring to Fig. 3, at time t_0, u_s is sampled once at the bottom of the carrier wave. At the same time, the sampling value is compared with the carrier wave to generate a SPWM pulse to trigger the inverter power switches to form the output phase voltage u.

In Fig. 3, θ_1 and θ_2 are the edge angles of u based on (2):

$$\begin{cases} \theta_1 = -\dfrac{\pi}{2}(1 + M\sin(\omega_s t_0 + \varphi)) \\ \theta_2 = \dfrac{\pi}{2}(1 + M\sin(\omega_s t_0 + \varphi)) \end{cases} \tag{2}$$

where $M = U_m / V_{rm}$.

Thus, u in one switching cycle is given as (3):

$$u = \begin{cases} -\dfrac{U_{dc}}{2} & -\pi \le \omega_c t < \theta_1, \theta_2 < \omega_c t \le \pi \\ \dfrac{U_{dc}}{2} & \theta_1 \le \omega_c t \le \theta_2 \end{cases} \tag{3}$$

Expanding u into the Fourier series, and letting $t = t_0$ yields:

$$u = \frac{MU_{dc}}{2}\sin(\omega_s t + \varphi) + \sum_{n=1}^{\infty}\left\{\frac{2U_{dc}}{n\pi} \times \left[\sin\frac{n\pi}{2} \times \cos\left(\frac{n\pi M}{2}\sin(\omega_s t + \varphi)\right) + \cos\frac{n\pi}{2} \times \sin\left(\frac{n\pi M}{2}\sin(\omega_s t + \varphi)\right)\right] \times \cos(n\omega_c t)\right\} \tag{4}$$

It can be seen from (4) that u consists of two parts, which are denoted here as u_m and u_n:

$$u_m = \frac{MU_{dc}}{2}\sin(\omega_s t + \varphi) \tag{5}$$

$$u_{\mathrm{n}}=\sum_{n=1}^{\infty}\left\{\frac{2U_{\mathrm{dc}}}{n\pi}\times\left[\sin\frac{n\pi}{2}\times\cos\left(\frac{n\pi M}{2}\sin(\omega_s t+\varphi)\right)+\cos\frac{n\pi}{2}\times\sin\left(\frac{n\pi M}{2}\sin(\omega_s t+\varphi)\right)\right]\times\cos(n\omega_{\mathrm{c}}t)\right\} \tag{6}$$

Analyzing (6), u_{m} is independent from the carrier frequency ω_{c}, and is mainly associated with u_{s}. Therefore, u_{m} may be called the low-frequency modulation component. In addition, u_{n} can be called the high-frequency switching component because it also depends on ω_{c} in addition to u_{s}.

IV. The SPWM High-frequency Circulating Current Characteristics of Parallel Systems

A. Mathematical Modeling of High-frequency Circulating Currents

Fig. 4 shown a high-frequency single-phase equivalent circuit of the parallel system.

In Fig. 4, $\boldsymbol{U}_{\mathrm{n1}}$ and $\boldsymbol{U}_{\mathrm{n2}}$ represent the high-frequency switching harmonic voltage vectors of module 1 and module 2, respectively; Z_{L} is the connection impedance of each module; $\boldsymbol{I}_1$, $\boldsymbol{I}_2$ and $\boldsymbol{I}_{\mathrm{s}}$ are the current vectors of each module and the parallel system; and the grid equivalent impedance is defined as Z_{s} which corresponds to R_{g} and L_{g}.

According to Fig. 4, $\boldsymbol{I}_1$, $\boldsymbol{I}_2$ and $\boldsymbol{I}_{\mathrm{s}}$ can be derived as follows:

$$\begin{cases}\boldsymbol{I}_1=\dfrac{\boldsymbol{U}_{\mathrm{n1}}}{Z_L+2Z_s}+\dfrac{Z_s\times(\boldsymbol{U}_{\mathrm{n1}}-\boldsymbol{U}_{\mathrm{n2}})}{Z_L(Z_L+2Z_s)}\\ \boldsymbol{I}_2=\dfrac{\boldsymbol{U}_{\mathrm{n2}}}{Z_L+2Z_s}+\dfrac{Z_s\times(\boldsymbol{U}_{\mathrm{n2}}-\boldsymbol{U}_{\mathrm{n1}})}{Z_L(Z_L+2Z_s)}\\ \boldsymbol{I}_s=\dfrac{\boldsymbol{U}_{\mathrm{n1}}+\boldsymbol{U}_{\mathrm{n2}}}{Z_L+2Z_s}\end{cases} \tag{7}$$

Analyzing (7), both $\boldsymbol{I}_1$ and $\boldsymbol{I}_2$ consist of two components, which are defined as:

$$\boldsymbol{I}_1=\boldsymbol{I}_{11}+\boldsymbol{I}_{12},\quad \boldsymbol{I}_2=\boldsymbol{I}_{22}+\boldsymbol{I}_{21} \tag{8}$$

where $\boldsymbol{I}_{11}=\dfrac{\boldsymbol{U}_{\mathrm{n1}}}{Z_L+2Z_s}$, $\boldsymbol{I}_{12}=\dfrac{Z_s\times(\boldsymbol{U}_{\mathrm{n1}}-\boldsymbol{U}_{\mathrm{n2}})}{Z_L(Z_L+2Z_s)}$, $\boldsymbol{I}_{22}=\dfrac{\boldsymbol{U}_{\mathrm{n2}}}{Z_L+2Z_s}$, and $\boldsymbol{I}_{21}=\dfrac{Z_s\times(\boldsymbol{U}_{\mathrm{n2}}-\boldsymbol{U}_{\mathrm{n1}})}{Z_L(Z_L+2Z_s)}$.

$\boldsymbol{I}_{12}$ and $\boldsymbol{I}_{21}$ are associated with the voltage difference $\Delta\boldsymbol{U}_{\mathrm{n}}=\boldsymbol{U}_{\mathrm{n1}}-\boldsymbol{U}_{\mathrm{n2}}$. In addition, $\boldsymbol{I}_{12}=-\boldsymbol{I}_{21}$. Obviously, $\boldsymbol{I}_{12}$ and $\boldsymbol{I}_{21}$ are the high-frequency harmonic circulating currents caused by the interaction of $\boldsymbol{U}_{\mathrm{n1}}$ and $\boldsymbol{U}_{\mathrm{n2}}$.

B. Formation Mechanism and Distribution Characteristics of the Circulating Currents and Their Impact on Parallel Systems

1) Formation Mechanism and Distribution Characteristics

Assuming that the phase lag of the SPWM carrier wave of module 2 compared with module 1 is φ_{c}, where $0\le\varphi_{\mathrm{c}}<2\pi$, the voltage difference Δu_{n} can be obtained using (6).

$$\Delta u_{\mathrm{n}}=u_{\mathrm{n1}}-u_{\mathrm{n2}}=\sum_{n=1}^{\infty}\left\{\frac{2U_{\mathrm{dc}}}{n\pi}\times\left[\sin\frac{n\pi}{2}\times\cos\left(\frac{n\pi M}{2}\sin(\omega_s t+\varphi)\right)+\cos\frac{n\pi}{2}\times\sin\left(\frac{n\pi M}{2}\sin(\omega_s t+\varphi)\right)\right]\times\left[\cos(n\omega_{\mathrm{c}}t)-\cos(n(\omega_{\mathrm{c}}t+\varphi_{\mathrm{c}}))\right]\right\} \tag{9}$$

Analyzing the expression $\cos(n\omega_c t)-\cos(n(\omega_c t+\varphi_c))$ in (9), the following conclusions can be drawn. Only when the SPWM carrier wave of module 1 is synchronous with module 2, namely $\varphi_{\mathrm{c}}=0$, there is $\Delta u_{\mathrm{n}}=0$, and thus $i_{12}=i_{21}=0$. Otherwise, when $\varphi_{\mathrm{c}}\neq0$, the high-frequency circulating currents i_{12} ($=i_{21}$) are produced due to $\Delta u_{\mathrm{n}}\neq0$.

Analyzing (9), when n is even, $\sin(n\pi/2)=0$; and when n is odd, $\cos(n\pi/2)=0$. Therefore, (9) can be further simplified as:

$$\Delta u_{\mathrm{n}}=\sum_{n=1}^{\infty}\left\{\left[(-1)^{(n-1)}\times\frac{4U_{\mathrm{dc}}}{(2n-1)\pi}\times\sin(\frac{2n-1}{2}\varphi_{\mathrm{c}})\times\cos\left(\frac{(2n-1)\pi M}{2}\sin(\omega_S t+\varphi)\right)\times\sin\left((2n-1)(\omega_{\mathrm{c}}t+\frac{\varphi_{\mathrm{c}}}{2})\right)\right]+\left[(-1)^{n}\times\frac{2U_{\mathrm{dc}}}{n\pi}\times\sin(n\varphi_{\mathrm{c}})\times\sin\left(n\pi M\sin(\omega_s t+\varphi)\right)\times\sin\left(2n(\omega_{\mathrm{c}}t+\frac{\varphi_{\mathrm{c}}}{2})\right)\right]\right\} \tag{10}$$

To thoroughly study the harmonic circulating currents characteristics, Bessel functions are introduced:

$$\begin{cases}\sin(x\sin\theta)=2\sum_{l=1}^{\infty}J_{2l-1}(x)\sin(2l-1)\theta\\ \cos(x\sin\theta)=J_0(x)+2\sum_{l=1}^{\infty}J_{2l}(x)\cos 2l\theta\end{cases} \tag{11}$$

Substituting (11) into (10), Δu_{n} may be given as (12).

According to (12), the frequency spectral distribution of the high-frequency harmonic circulating currents is primarily comprised of two portions:

$$\Delta u_{\mathrm{n}}=\sum_{n=1}^{\infty}\left\{\left\{(-1)^{(n-1)}\times\frac{4U_{\mathrm{dc}}}{(2n-1)\pi}\times\sin(\frac{2n-1}{2}\varphi_{\mathrm{c}})\times\left[J_0(\frac{(2n-1)\pi M}{2})\times\sin((2n-1)\omega_{\mathrm{c}}t+\frac{2n-1}{2}\varphi_{\mathrm{c}}))+\sum_{l=1}^{\infty}\left[J_{2l}(\frac{(2n-1)\pi M}{2})\times\left[\sin((2l\omega_s+(2n-1)\omega_{\mathrm{c}})t+2l\varphi+\frac{2n-1}{2}\varphi_{\mathrm{c}})-\sin((2l\omega_s-(2n-1)\omega_{\mathrm{c}})t+2l\varphi-\frac{2n-1}{2}\varphi_{\mathrm{c}})\right]\right]\right\}+\left\{(-1)^{n}\times\frac{2U_{\mathrm{dc}}}{n\pi}\times\sin(n\varphi_{\mathrm{c}})\times\sum_{l=1}^{\infty}\left[J_{2l-1}(n\pi M)\times\left[\cos(((2l-1)\omega_s-2n\omega_{\mathrm{c}})t+(2l-1)\varphi-n\varphi_{\mathrm{c}})-\cos(((2l-1)\omega_s+2n\omega_{\mathrm{c}})t+(2l-1)\varphi+n\varphi_{\mathrm{c}})\right]\right]\right\}\right\} \tag{12}$$

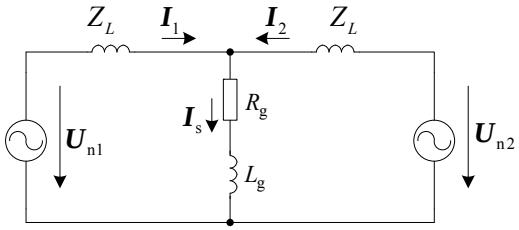

Fig. 4. The high-frequency single-phase equivalent circuit of the parallel system.

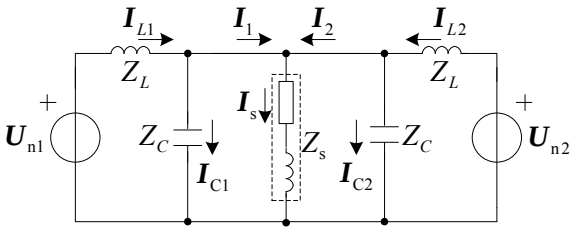

Fig. 5. The high-frequency single-phase equivalent circuit based on the LC-type filter.

First, the harmonic frequencies are $(2n\text{-}1)\omega_c$ and $(2n\text{-}1)\omega_c \pm 2l\omega_s$. In this case, the harmonic distribution is near the odd multiples of the carrier frequency $(2n\text{-}1)\omega_c$, and the side frequencies are the even multiples of the modulation wave frequency $2l\omega_s$.

Second, the harmonic frequencies are $2n\omega_c \pm (2l\text{-}1)\omega_s$. In this case, the harmonic distribution is around the even multiples of the carrier frequency $2n\omega_c$, and the side frequencies are the odd multiples of the modulation wave frequency $(2l\text{-}1)\omega_s$.

Based on the above analysis, the distribution characteristics of the harmonic circulating currents can be obtained. The high-frequency harmonic circulating currents are in an odd distribution around the n times the carrier frequency $n\omega_s$, where n = 1, 2, 3, ….

2) Impacts on the parallel system

On the basis of Fig. 4, the combination of (7) and (8) yields the following relational expression:

$$\boldsymbol{I}_s = \boldsymbol{I}_1 + \boldsymbol{I}_2 = \boldsymbol{I}_{11} + \boldsymbol{I}_{22} \tag{13}$$

Formula (13) show that, $\boldsymbol{I}_s$ does not contain $\boldsymbol{I}_{12}$ or $\boldsymbol{I}_{21}$. In other words, the harmonic circulating currents have no influence on the parallel system.

Below, a brief analysis of the impact of SPWM carrier phase shifting on the high-frequency switching harmonics in a parallel system will be presented.

According to (6), the sum of the two high-frequency harmonic voltages of each module denoted as Σu_n is given by:

$$\sum u_n = u_{n1} + u_{n2} = \sum_{n=1}^{\infty}\left\{\frac{2U_{dc}}{n\pi}\times\left[\sin\frac{n\pi}{2}\times\cos\left(\frac{n\pi M}{2}\sin(\omega_s t+\varphi)\right)+\cos\frac{n\pi}{2}\times \sin\left(\frac{n\pi M}{2}\sin(\omega_s t+\varphi)\right)\right]\times\left[\cos(n\omega_c t)+\cos(n(\omega_c t+\varphi_c))\right]\right\} \tag{14}$$

The conclusions can be obtained from the expression $\cos(n\omega_c t) + \cos(n(\omega_c t + \varphi_c))$ in (14):

First, when the carrier waves of all the modules are synchronous, namely φ_c=0, the switching harmonics in the parallel system is just twice that of a single module. In this situation, the switching harmonics in the parallel system reach the maximum. However, according to (9), the switching harmonic circulating currents between the modules are zero.

Second, when $\varphi_c=\pi$, $\cos(n\omega_c t) + \cos(n(\omega_c t + \varphi_c))$ can be simplified as:

$$\cos(n\omega_c t) + \cos(n(\omega_c t + \varphi_c)) = \begin{cases} 2\cos(n\omega_c t), & n=2,4,6,\cdots \\ 0, & n=1,3,5,\cdots \end{cases}$$

By the above equation, (14) can be converted as:

$$\sum u_n = \sum_{k=1}^{\infty}\left\{(-1)^k\times\frac{2U_{dc}}{k\pi}\times\sin\left(k\pi M\sin(\omega_s t+\varphi)\right)\times\cos(2k\omega_c t)\right\} \tag{15}$$

Comparing (14) and (15) shows that when $\varphi_c=\pi$, the harmonic currents of the odd multiples of the carrier frequency ω_c are eliminated in parallel systems. In this case, the harmonic content in parallel systems reaches the minimum. However, the harmonic circulating currents between the modules are up to the maximum based on (9).

Summarizing the above two points it can be seen that for modular inverters, the carrier phase shifting of SPWM can prevent some of the switching harmonics of each module from flowing into the parallel system. However, this also results in switching circulating currents among the modules.

V. Influences of an OF on the Circulating Currents

The common OF in an inverter includes LC-type filter, LCL-type filter, 2-order high-pass filter and so on. Taking an LC-type filter and an LCL-type filter as two examples, this paper analyses their impacts on high-frequency harmonic circulating currents.

A. Influences of an LC-type OF

A high-frequency single-phase equivalent circuit of a double-module VSI based on an LC-type filter is shown in Fig. 5.

In Fig. 5, Z_C is the capacitive reactance of the OF. In module 1, $\boldsymbol{I}_{L1}$ is the device-side output current between the OF and the device, $\boldsymbol{I}_{C1}$ is the capacitor current of the OF, and $\boldsymbol{I}_1$ is the system-side output current near the parallel system. The same definitions of $\boldsymbol{I}_{L2}$, $\boldsymbol{I}_{C1}$ and $\boldsymbol{I}_1$ are used in module 2.

According to Fig. 5, $\boldsymbol{I}_{L1}$, $\boldsymbol{I}_{C1}$, $\boldsymbol{I}_1$, $\boldsymbol{I}_{L2}$, $\boldsymbol{I}_{C2}$, $\boldsymbol{I}_2$ and $\boldsymbol{I}_s$ can be derived. Due to the symmetry of the circuit in Fig. 5, only the expressions of $\boldsymbol{I}_{L1}$, $\boldsymbol{I}_{C1}$, $\boldsymbol{I}_1$, and $\boldsymbol{I}_s$ are listed as follows:

$$\begin{cases} \boldsymbol{I}_{L1} = \dfrac{(2Z_s+Z_c)\times\boldsymbol{U}_{n1}}{2Z_LZ_s+2Z_cZ_s+Z_cZ_L} + \dfrac{Z_sZ_c\times(\boldsymbol{U}_{n1}-\boldsymbol{U}_{n2})}{Z_L(2Z_LZ_s+2Z_cZ_s+Z_cZ_L)} \\ \boldsymbol{I}_{C1} = \dfrac{Z_s}{2Z_LZ_s+2Z_cZ_s+Z_cZ_L}\times(\boldsymbol{U}_{n1}+\boldsymbol{U}_{n2}) \\ \boldsymbol{I}_{1} = \dfrac{Z_c\times\boldsymbol{U}_{n1}}{2Z_LZ_s+2Z_cZ_s+Z_cZ_L} + \dfrac{(Z_L+Z_C)Z_s\times(\boldsymbol{U}_{n1}-\boldsymbol{U}_{n2})}{Z_L(2Z_LZ_s+2Z_cZ_s+Z_cZ_L)} \\ \boldsymbol{I}_{s} = \dfrac{Z_c}{2Z_LZ_s+2Z_cZ_s+Z_cZ_L}\times(\boldsymbol{U}_{n1}+\boldsymbol{U}_{n2}) \end{cases} \tag{16}$$

In a similar way, in accordance with (8), these parts, which are associated with the voltage difference $\Delta\boldsymbol{U}_n$ in $\boldsymbol{I}_{L1}$ and $\boldsymbol{I}_1$, are the high-frequency harmonic circulating currents, which are defined as:

$$\begin{cases} \boldsymbol{I}_{L12} = \dfrac{Z_sZ_c\times(\boldsymbol{U}_{n1}-\boldsymbol{U}_{n2})}{Z_L(2Z_LZ_s+2Z_cZ_s+Z_cZ_L)} \\ \boldsymbol{I}_{12} = \dfrac{(Z_L+Z_c)Z_s\times(\boldsymbol{U}_{n1}-\boldsymbol{U}_{n2})}{Z_L(2Z_LZ_s+2Z_cZ_s+Z_cZ_L)} \end{cases} \tag{17}$$

The harmonic distribution characteristics of $\boldsymbol{I}_{L12}$ and $\boldsymbol{I}_{12}$ are consistent with $\boldsymbol{I}_{12}$ or $\boldsymbol{I}_{21}$, which are not analyzed in length here. Based on (17), under the condition of Δu_n=0, namely, when the SPWM carrier wave of module 1 is synchronized with module 2, i_{12}=i_{21}=0. This section mainly focuses on the impacts of the OF on the existing harmonic circulating currents.

Converting (17) into the form of a transfer function yields:

$$\begin{cases} I_{L12}(s)=G_{L12}(s)\times(U_{n1}(s)-U_{n2}(s)) \\ I_{12}(s)=G_{12}(s)\times(U_{n1}(s)-U_{n2}(s)) \end{cases} \tag{18}$$

where:

$$G_{L12}(s) = \frac{L_gs+R_g}{2L^2L_gC_fs^4+2L^2R_gC_fs^3+(2LL_g+L^2)s^2+2LR_gs}$$

$$G_{12}(s) = \frac{LL_gC_fs^3+LR_gC_fs^2+L_gs+R_g}{2L^2L_gC_fs^4+2L^2R_gC_fs^3+(2LL_g+L^2)s^2+2LR_gs}$$

Similarly, defining the transfer function G(s) for I_{12} in equation (8) yields:

$$G(s) = \frac{L_gs+R_g}{L(L+2L_g)s^2+2R_gLs} \tag{19}$$

Bode diagrams of G(s), G_{L12}(s) and G_{12}(s) are given in Fig. 6, and the system parameters are presented in Table I.

Fig. 6 shows that, there were obvious resonances in G_{L12}(s) and G_{12}(s), and the phase angle decreased sharply at the resonance frequency. In particular, the phase margin of G_{L12}(s) was close to -90° when its resonance amplitude fell across 0dB. Thus, the system entered an unstable state. In addition, by comparing the amplitude-frequency characteristics between G(s) and G_{12}(s), it can be seen that there was no significant suppression effect on the high-frequency circulating currents from the LC-type OF.

B. Influences of an LCL-type OF

A high-frequency single-phase equivalent circuit based on an LCL-type filter is shown in Fig. 7.

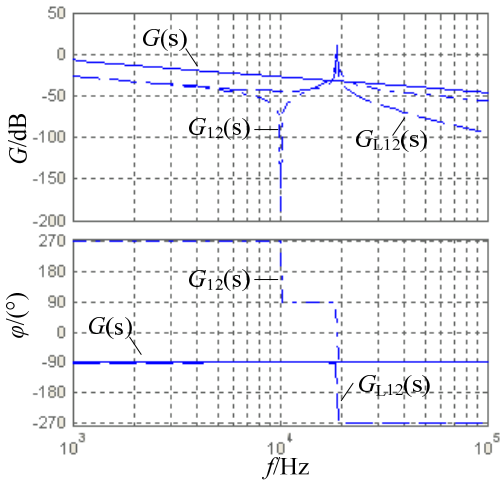

Fig. 6. The Bode diagram of G(s), G_{L12}(s) and G_{12}(s) in Equ. (18).

TABLE I
SYSTEM PARAMETERS

Parameters	Value
DC-side Capacitor of the modular inverter, C	5000 μF
Inductor of the OF, L	0.5 mH
Capacitor of the OF, C_f	0.5 μF
Grid equivalent reactance L_g and resistance R_g	0.1 mH, 20 mΩ
Switching frequency, f_s	10 kHz

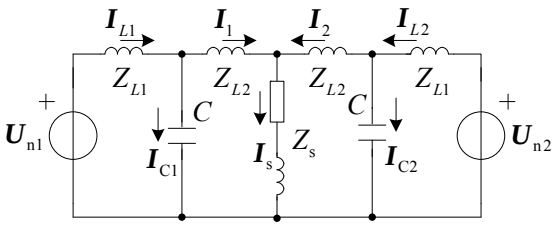

Fig. 7. The high-frequency single-phase equivalent circuit based on the LCL-type filter.

In Fig. 7, Z_{L1} and Z_{L2} are the device-side inductive reactance and the system-side inductive reactance of the LCL OF, respectively. For the other parameters refer to Fig. 5.

Similarly, according to Fig. 7, $\boldsymbol{I}_{L1}$, $\boldsymbol{I}_{C1}$, $\boldsymbol{I}_1$ and $\boldsymbol{I}_s$ can be derived as follows:

$$\begin{cases} \boldsymbol{I}_{L1} = \dfrac{(A+B+Z_c^2)\times\boldsymbol{U}_{n1}}{(Z_{L1}+Z_c)\times(A+B)} + \dfrac{Z_c^2B\times(\boldsymbol{U}_{n1}-\boldsymbol{U}_{n2})}{(Z_{L1}+Z_c)\times(A^2-B^2)} \\ \boldsymbol{I}_{C1} = \dfrac{(A^2-B^2-Z_{L1}Z_cA)\times\boldsymbol{U}_{n1}+Z_{L1}Z_cB\times\boldsymbol{U}_{n2}}{(Z_{L1}+Z_c)\times(A^2-B^2)} \\ \boldsymbol{I}_{1} = \dfrac{Z_c\times\boldsymbol{U}_{n1}}{A+B} + \dfrac{Z_cB\times(\boldsymbol{U}_{n1}-\boldsymbol{U}_{n2})}{(A^2-B^2)} \\ \boldsymbol{I}_{s} = \dfrac{Z_c}{A+B}\times(\boldsymbol{U}_{n1}+\boldsymbol{U}_{n2}) \end{cases} \tag{20}$$

where:

$$A = Z_{L1}Z_c + Z_{L1}Z_{L2} + Z_{L2}Z_c + Z_{L1}Z_s + Z_cZ_s$$

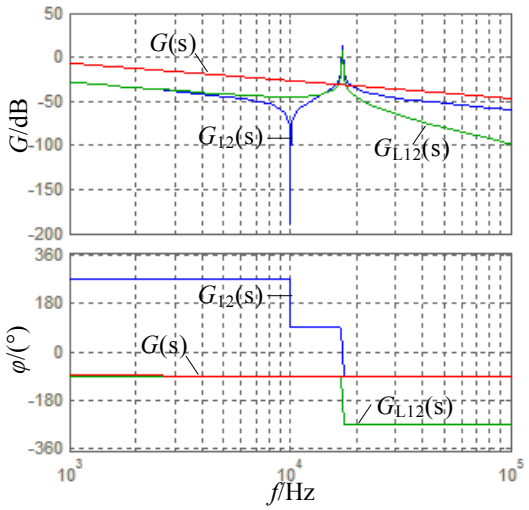

Fig. 8. The Bode diagram of G(s), G_{L12}(s) and G_{12}(s) in Equ. (22).

$$B = Z_{L1}Z_s + Z_cZ_s$$

In a similar way, in accordance with (17), the high-frequency harmonic circulating currents which are associated with the voltage difference $\Delta \boldsymbol{U}_n$ in $\boldsymbol{I}_{L1}$ and $\boldsymbol{I}_1$ are defined as:

$$\begin{cases} \boldsymbol{I}_{L12} = \dfrac{Z_c^2 B}{(Z_{L1}+Z_c)\times(A^2-B^2)} \times (\boldsymbol{U}_{n1} - \boldsymbol{U}_{n2}) \\ \boldsymbol{I}_{12} = \dfrac{Z_c B}{(A^2-B^2)} \times (\boldsymbol{U}_{n1} - \boldsymbol{U}_{n2}) \end{cases} \tag{21}$$

Convert (21) into the form of a transfer function, which is similar to (18), where G_{L12}(s) and G_{12}(s) are as follows:

$$\begin{cases} G_{L12}(s) = \dfrac{1}{L_1Cs^2+1} \times \dfrac{1}{L_1L_2Cs^3+(L_1+L_2)s} \times \\ \dfrac{L_1L_gCs^3+L_1R_gCs^2+L_gs+R_g}{(L_1L_2C+2L_1L_gC)s^3+2L_1R_gCs^2+(L_1+L_2+2L_g)s+2R_g} \\ G_{12}(s) = \dfrac{1}{L_1L_2Cs^3+(L_1+L_2)s} \times \\ \dfrac{L_1L_gCs^3+L_1R_gCs^2+L_gs+R_g}{(L_1L_2C+2L_1L_gC)s^3+2L_1R_gCs^2+(L_1+L_2+2L_g)s+2R_g} \end{cases} \tag{22}$$

Bode diagrams of G(s), G_{L12}(s) and G_{12}(s) are given in Fig. 8. L_1 and L_2 are set to 0.5mH and 0.06mH, respectively. For the other parameters refer to Table I.

By comparing Fig. 8 and Fig. 6, it can be seen that the resonance characteristics of i_{L12} and i_{12}, which are based on an LCL-type OF, are the same as those of i_{L12} and i_{12}, which are based on an LC-type OF, except for a difference in the resonance frequency. In other words, like the LC filter, the LCL filter did not have a significant suppression effect on the high-frequency circulating currents. Furthermore, the probability of resonance may be enhanced.

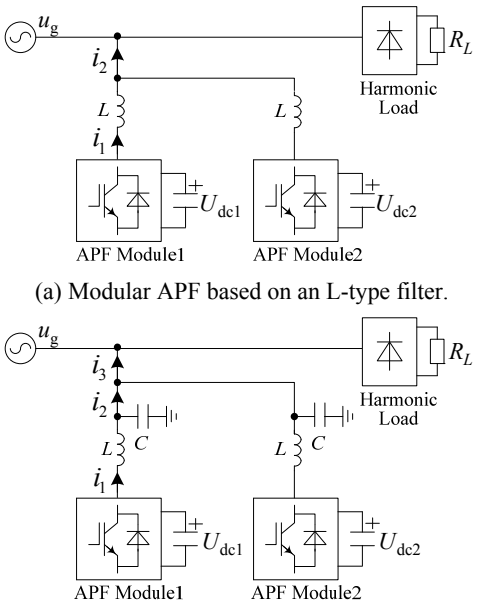

(a) Modular APF based on an L-type filter.

(b) Modular APF based on an LC-type filter.

Fig. 9. The simplified experimental circuit structure.

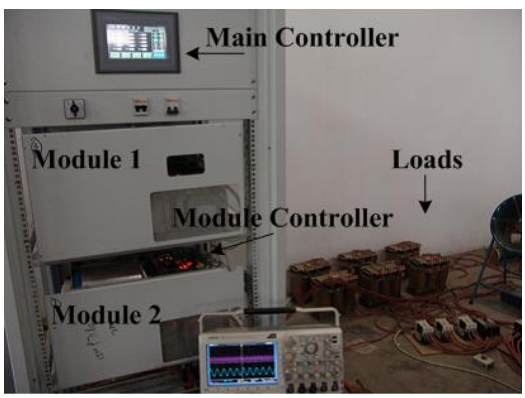

Fig. 10. The picture of the experimental device.

VI. Experimental Results

A. Design of the Experimental Circuit

A modular active power filter (APF) that has the same circuit structure as Fig. 2 is considered for the experiment performed in this paper. In addition, a three-phase diode rectifier with a resistance load R_L is considered for the harmonic load.

Due to the fact that the LCL-type OF and the LC-type OF have the same resonance characteristics, the LC-type OF is selected for the experiment. A simplified experimental circuits are shown in Fig. 9. In Fig. 9, an L-type OF is installed for circuit (a) and an LC-type OF is installed for circuit (b) to study the influences of an OF on the circulating currents through a comparative analysis. A picture of the experimental device is shown in Fig. 10.

B. Design of the Experimental Control System

The experimental control system is shown in Fig. 11.

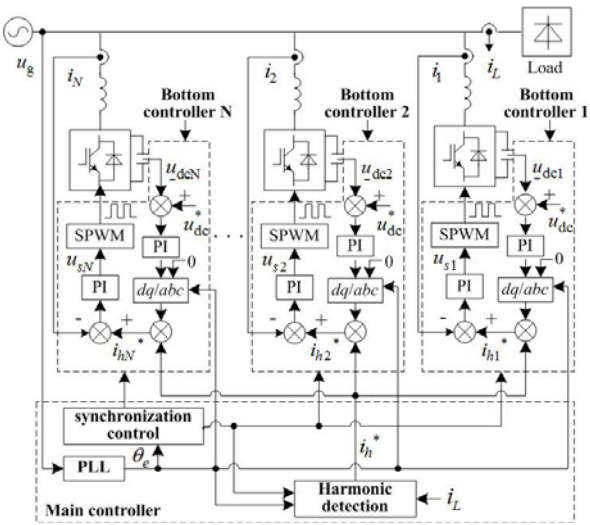

Fig. 11. The structure of the control system of modular APF.

In Fig. 11, N is the number of APF modules, and N=2 in this experiment. θ_e is the phase information of u_g which is generated by the digital phase-locked loop (PLL), U_{dc}* is the command value for the DC voltage of each module, i_{hk}^* is the harmonic compensation instruction current, and u_{sk} is the output modulated voltage of each current controller, where k=1, 2, ⋯, and N.

Referring to Fig. 11, the distributed control mode is considered for the experimental control system which is composed of two parts: the main control and bottom control of each module. The main controller mainly achieves the coordinated control functions, such as the synchronization control, including the SPWM carrier synchronization and carrier phase-shift control, the harmonic current detection and distribution, and the fault tolerance control. The bottom controllers complete their control functions under the coordinated control of the main controller, and the DC voltage outer-loop control and current tracking inner-loop control are mainly involved in each bottom controller.

C. Experiment Analysis

In the experimental system, an AC source is supplied by a 10kV/0.4kV transformer. Accordingly, the power supply voltage u_g is 400V. In addition, R_L is set to 10Ω, U_{dc}* is set to 800V, and for the other parameters refer to Table I.

1) Experiment with circuit (a) in Fig. 9:

According to the experimental circuit (a) in Fig. 9, i_1 is the output current of module 1, and i_2 is the summed current of the parallel system.

Fig. 12 shows the current waveforms of i_1 and i_2 when the SPWM carrier wave of module 1 is synchronous with module 2. Meanwhile Fig. 13 shows them when the carrier phase shifting of the SPWM between module 1 and module 2 is set to half of the switching cycle T_c. The experimental results are as follows:

First, comparing the two current waveforms of i_1 in Fig. 12

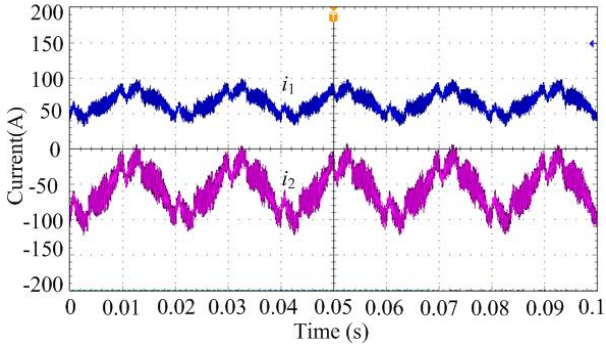

Fig. 12. The current waveforms of i_1 and i_2 when the SPWM carrier waves of the two modules are synchronous.

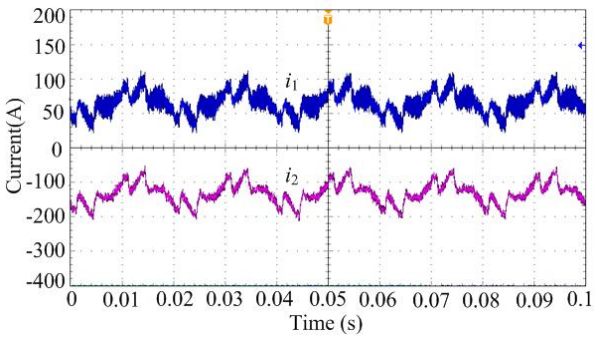

Fig. 13. The current waveforms of i_1 and i_2 on the condition that the carrier phase shifting of SPWM between the two modules is set by half of the switching cycle T_c.

and Fig. 13, it can be seen that there are more high-frequency harmonic components in the current i_1 shown in Fig. 13. However, they do not exist in the current i_2 shown in Fig. 13. Obviously, the harmonic current components are the harmonic circulating currents that match the currents i_{12} and i_{21} in equation (8). These experimental result verify the theoretical analysis conclusion above. They show that the carrier phase shifting of the SPWM of each module is the major cause of the harmonic circulating currents.

Second, comparing the current waveforms of i_2 in Fig. 12 and Fig. 13, it can be clearly seen that the high-frequency harmonic components in i_2 in Fig. 13 are far less than those in Fig. 12. These experimental results are consistent with the theoretical analysis conclusion. They show that some of the high-frequency switching harmonic currents of each module can be eliminated by the carrier phase-shifted SPWM (CPS-SPWM) technique. However, this also results in switching circulating currents among the modules. In addition, these experimental results further show that the circulating currents between the modules have no effect on the parallel system currents.

2) Experiment with circuit (b) in Fig. 9:

According to the experimental circuit (b) in Fig. 9, i_1 is the output current before the LC-type OF (between the inverter and the LC-type OF), i_2 is output current after the LC-type OF, and i_3 is the summed current of the parallel system.

Fig. 14 has the same experimental conditions of the SPWM

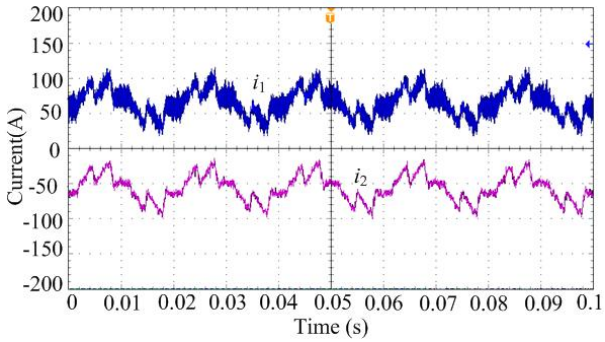

Fig. 14. The current waveforms of i_1 and i_2 when the SPWM carrier waves of the two modules with the LC-type OF are synchronous.

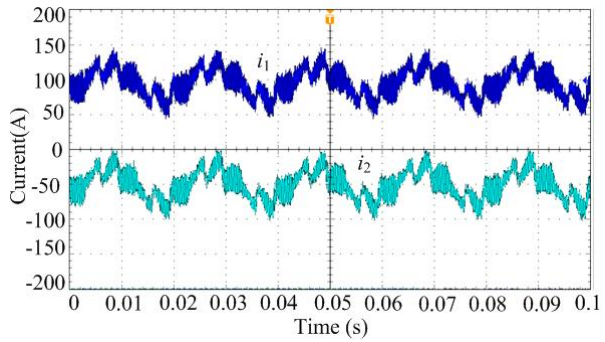

Fig. 15. The current waveforms of i_1 and i_2 on the condition that the carrier phase shifting of SPWM between the two modules with the LC-type OF is set by half of the switching cycle T_c.

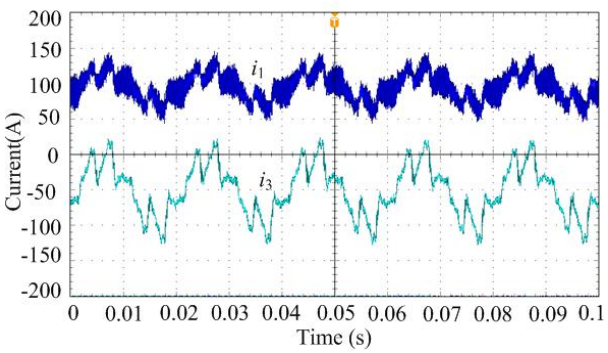

Fig. 16. The current waveforms of i_1 and i_3 on the condition that the carrier phase shifting of SPWM between the two modules with the LC-type OF is set by half of the switching cycle T_c.

carrier phase as Fig. 12. In addition, Fig. 15 and Fig. 16 have the same experimental conditions as Fig. 13. The experimental results are as follows:

First, according to Fig. 14, when the SPWM carrier wave of each module is synchronous, the LC-type OF can effectively filter most of the high-frequency switching harmonic currents.

Second, according to Fig. 15, when the SPWM carrier phase of each module is shifted, the LC-type OF cannot filter the high-frequency switching harmonic currents. In fact, the high-frequency harmonic currents that cannot be filtered by the OF are exactly the high-frequency harmonic circulating currents. These experimental results show that the OF has no obvious inhibitory effect on the high-frequency harmonic circulating currents, which is in accordance with the theoretical analysis conclusions above.

In addition, Fig. 16 shows that high-frequency harmonic circulating currents do not flow into the parallel system. Furthermore, comparing i_2 in Fig. 13 with i_3 in Fig. 16, it can be seen that the non-circulating components of the high-frequency harmonic circulating currents are found to be inhibited by the LC-type OF.

VII. Conclusions

Through theoretical analysis, simulations and experimental results, the formation mechanism and distribution characteristics of the SPWM high-frequency harmonic circulating currents in a modular inverter and their impact on parallel systems were analyzed in detail. Furthermore, by taking an LC-type OF as an example, the influences of an OF on the circulating currents were studied in this paper. The research results are summarized as follows:

First, the carrier phase shifting of the SPWM of each module is the major cause of SPWM high-frequency harmonic circulating currents, and the circulating currents are in an odd distribution around n-times the carrier frequency $n\omega_s$, where $n = 1, 2, 3, \ldots$.

Second, harmonic circulating currents do not flow into parallel systems. In other words, the harmonic circulating currents have no influence on parallel systems.

Third, an OF can effectively suppress the non-circulating components of high-frequency harmonic currents. However, it is ineffective in suppressing circulation components, and reduces system stability.

Moreover, some of the high-frequency switching harmonic currents of each module can be eliminated by the CPS-SPWM technique. However, this also results in switching circulating currents among the modules.

Acknowledgment

The authors wish to thank the National Natural Science Foundation of China (51477030), the Natural Science Foundation of the Jiangsu Higher Education Institutions of China (14KJB470008), the Research Institutes Association Innovative Program of Jiangsu Province (BY2014127-15 and BY2016076-14), China Postdoctoral Science Foundation (2016M591739), and Taizhou science and technology support program (TS201629).

References

[1] K. Ilves, A. Antonopoulos, L. Harnefors, S. Norrga, and H. P. Nee, "Circulating current control in modular multilevel converters with fundamental switching frequency," in 7th

International Power Electronics and Motion Control Conference (IPEMC), pp. 249-256, Jun. 2012.
[2] Y. Zhang, S. Duan, Y. Kang, and J. Chen, "The restrain of harmonic circulating currents between parallel inverters," in *CES/IEEE 5th International Power Electronics and Motion Control Conference (IPEMC)*, pp. 1-5, Aug. 2006.
[3] J. A. P. Lopes, C. L. Moreira, and A. G. Madureira, "Defining control strategies for microgrid island operation," *IEEE Trans. Power Syst.*, Vol. 21, No. 2, pp. 916-924, May 2006.
[4] Y. A. R. I. Mohamed and E. F. El Saadany, "Adaptive decentralized droop controller to preserve power sharing stability of paralleled inverters in distributed generation microgrids," *IEEE Trans. Power Electron.*, Vol. 23, No. 6, pp. 2806-2816, Nov. 2008.
[5] Z. He and Y. Xing, "Distributed control for UPS modules in parallel operation with rms voltage regulation," *IEEE Trans. Ind. Electron.*, Vol. 55, No. 8, pp. 2860-2869, Aug. 2008.
[6] X. Sun, Y. S. Lee, and D. Xu, "Modeling, analysis, and implementation of parallel multi-inverter systems with instantaneous average-current-sharing scheme," *IEEE Trans. Power Electron.*, Vol. 18, No. 3, pp. 844-856, May 2003.
[7] L. Chen, L. Xiao, C. Gong, and Y. Yan, "Circulating current's characteristics analysis and the control strategy of parallel system based on double close-loop controlled VSI," in *IEEE 35th Annual Power Electronics Specialists Conference (PESC)*, pp. 4791-4797, Jun. 2004.
[8] K. D. Brabandere, B. Bolsens, J. V. D. Keybus, A. Woyte, J. Driesen, and R. Belmans, "A voltage and frequency droop control method for parallel inverters," *IEEE Trans. Power Electron.*, Vol. 22, No. 4, pp. 1107-1115, Jul. 2007.
[9] J. M. Guerrero, J. C. Vasquez, J. Matas, L. G. D. Vicuna, and M. Castilla, "Hierarchical control of droop-controlled ac and dc microgrids-a general approach toward standardization," *IEEE Trans. Ind. Electron.*, Vol. 58, No. 1, pp. 158-172, Jan. 2011.
[10] A. Tuladhar, H. Jin, T. Unger, and K. Mauch, "Control of parallel inverters in distributed AC power systems with consideration of line impedance effect," *IEEE Trans. Ind. Appl.*, Vol. 36, No. 1, pp. 131-138, Jan./Feb. 2000.
[11] F. Xu, B. Guo, Z. Xu, L. M. Tolbert, F. Wang, and B. J. Blalock, "SiC based current source rectifier paralleling and circulating current suppression," in *28th Annual IEEE Applied Power Electronics Conference and Exposition (APEC)*, pp. 402-409, Mar. 2013.
[12] X. Zhang, W. Zhang, J. Chen, and D. Xu, "Deadbeat control strategy of circulating currents in parallel connection system of three-phase PWM converter," *IEEE Trans. Energy Convers.*, Vol. 29, No. 2, pp. 406-417, Jun. 2014.
[13] T. Itkonen, J. Luukko, A. Sankala, T. Laakkonen, and R. Pollanen, "Modeling and analysis of the dead-time effects in parallel PWM two-level three-phase voltage-source Inverters," *IEEE Trans. Power Electron.*, Vol. 24, No. 11, pp. 2446-2455, Nov. 2009.
[14] J. B. Liu, H. Lin, and X. Qin, "Study on restraint of circulating current in parallel inverters system with SPWM modulation by adjusting phases of triangular carrier waves," in *2nd International Symposium on Instrumentation and Measurement, Sensor Network and Automation (IMSNA)*, pp. 477-480, Dec. 2013.
[15] X. Bao, F. Zhuo, B. Liu, and Y. Tian, "Suppressing switching frequency circulating current in parallel inverters with Carrier Phase-Shifted SPWM technique," in *IEEE International Symposium on Industrial Electronics (ISIE)*, pp. 555-559, May 2012.
[16] C. Xie, Y. Wang, X. Zhong, and G. Chen, "A novel active damping method for LCL-filter-based shunt active power filter," in *IEEE International Symposium on Industrial Electronics (ISIE)*, pp. 64-69, May 2012.
[17] D. Pan, X. Ruan, X. Wang, C. Bao, and W. Li, "Magnetic integration of an LCL filter for the single-phase grid-connected inverter," in *IEEE Energy Conversion Congress and Exposition (ECCE)*, pp. 573-578, Sep. 2012.

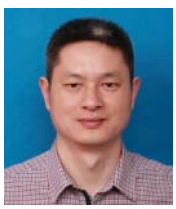

Sheng Xu was born in China, in 1976. He received his B.S. degree in Mechanical and Electronic Engineering from Nanjing Agricultural University, Nanjing, China, in 1999; his M.S. degree in Electrical Engineering from the Nanjing University of Science and Technology, Nanjing, China, in 2005; and his Ph.D. degree in Electrical Engineering from Southeast University, Nanjing, China, in 2010. In 2011, he joined the Department of Mechanical and Electrical Engineering, Taizhou University, Taizhou, China, where he has been working as an Associate Professor since 2013. His current research interests include power quality mitigation and high-power converters.

Zhendong Ji was born in Yancheng, China. He received his B.S. and Ph.D. degrees in Electrical Engineering from Southeast University, Nanjing, China, in 2007 and 2015, respectively. In 2015, he joined the School of Automation, Nanjing University of Science and Technology, Nanjing, China, where he is presently working as a Lecturer. His current research interests include cascade multilevel converters and solid-state transformers.